Experimental Study and Modeling of Radio Wave Propagation for IoT in Underground Wine Cellars

Original Scientific Paper

Snježana Rimac-Drlje*
J. J. Strossmayer University of Osijek,
Faculty of Electrical Engineering, Computer Science and Information Technology Osijek
Kneza Trpimira 2B, Osijek, Croatia
snjezana.rimac@ferit.hr

Tomislav Keser
J. J. Strossmayer University of Osijek,
Faculty of Electrical Engineering, Computer Science and Information Technology Osijek
Kneza Trpimira 2B, Osijek, Croatia
tomislav.keser@ferit.hr

Vanja Mandrić
J. J. Strossmayer University of Osijek,
Faculty of Electrical Engineering, Computer Science and Information Technology Osijek
Kneza Trpimira 2B, Osijek, Croatia
vanja.mandric@ferit.hr

Slavko Rupčić
J. J. Strossmayer University of Osijek,
Faculty of Electrical Engineering, Computer Science and Information Technology Osijek
Kneza Trpimira 2B, Osijek, Croatia
slavko.rupcic@ferit.hr

*Corresponding author

Abstract *– This paper presents the results of a study of radio wave propagation in underground wine cellars in the context of the optimal use of wireless communication systems for the application of the Internet of Things (IoT) in wine production environments. Electric field strength measurements were carried out in two subterranean line-of-sight (LOS) and non-line-of-sight (NLOS) conditions at 860 MHz, 2400 MHz, and 3600 MHz. The measured results were compared with predictions from seven existing propagation models, including site-general models (Free-space, ITU-R P.1238-13, ITU-R P.1411-12, ETSI TR 138 901 V16.1.0) and site-specific models (ITU-R P.1411-12, tunnel and knife-edge diffraction). Statistical analysis determined that the ITU-R P.1238-13 model, which estimates path loss in corridors, and the tunnel model have the best agreement with measurements in LOS conditions, with average Root Mean Square Error (RMSE) values of 2.8 dB and 3.56 dB, respectively. For the NLOS regions, the knife-edge diffraction model achieved the highest accuracy (average RMSE = 2.77 dB). Furthermore, based on the measurement results, the coefficients of the general path-loss model were adjusted to the data using the least-squares method, yielding RMSEs of 2.02 dB for LOS and 2.65 dB for NLOS conditions. The analysis showed that combining the ITU-R P.1238-13 or tunnel model for LOS conditions with a diffraction-based model for NLOS conditions provides a good basis for modeling radio propagation in subterranean wine cellars. These findings support the design of efficient and robust IoT communication networks in winery environments.*

Keywords: *Internet of Things (IoT), underground wine cellar, radio wave propagation, path loss modeling*

Received: October 16, 2025; Received in revised form: November 11, 2025; Accepted: November 12, 2025

1. INTRODUCTION

The application of smart technologies in production processes improves product quality while reducing energy consumption and conserving other essential resources. The application of sensors plays a major role in this, and the rapid progress of the Internet of Things (IoT), sensor technologies, and various communication solutions that enable sensor connectivity have created significant opportunities for the application of wireless sensor networks even in traditional industrial sectors such as wine production [1–6]. Due to the inherent variability of grapes, whose properties are influenced by meteorological conditions, soil composition, and agronomic practices during cultivation, the wine production process is not standardized and must be continually adapted to the current state of the must or wine. Consequently, continuous monitoring and measurement of production parameters are essential to identify potential deviations and take timely corrective actions. The collection and processing of various data requires reliable transmission of measurements to a centralized unit where predictive models developed using machine learning techniques can be used to predict the behavior of parameters and thus support process management and optimization [1-4].

Given that a large number of wine containers are typically distributed across a wide area, wireless communication is the most practical and efficient means of data transmission. Considering that the volume of transmitted data is relatively modest, robust communication systems such as LoRa or NB-IoT are suitable; however, WiFi-based solutions can also be acceptable alternatives. When designing a radio communication system, it is essential to select an appropriate model for estimating propagation losses of radio waves. Propagation models are intensively researched in different scenarios (indoor, outdoor, outdoor-to-indoor), and environments (urban, suburban, rural, indoor corridors/ rooms/multi-floor, tunnels), and for different frequencies, depending on the model's area of application [7-14]. However, there are only a few studies on radio wave propagation in basements with architectural features such as wine cellars, [15, 16].

Wine production facilities can generally be divided into two categories: traditional cellars and purpose-built structures. These two environments differ significantly in architectural design and construction materials, which in turn lead to variations in radio wave propagation behavior. This paper focuses on the propagation of radio waves in traditional wine cellars, which are typically characterized by their subterranean location, thick brick or stone walls, absence of windows, elongated corridors with low ceilings, and frequently vaulted structures. The high humidity commonly found in wine cellars influences the electromagnetic properties of the building materials [17], consequently affecting the absorption and reflection of electromagnetic waves. Moreover, the wine containers themselves have a distinctive impact on wave propagation, depending on their size, spatial arrangement, and material composition. Stainless steel tanks, which are widely used in modern wineries, act as reflectors of radio waves due to their high conductivity, and direct the reflections in a specific way because of their rounded shape. As additional causes of reflection and diffraction of radio waves, they make propagation conditions in the cellars even more complex.

Given the similar architectural characteristics, models developed for radio wave propagation in tunnels or corridors [18–22] represent potential candidates for modeling propagation losses in wine cellars. However, to the best of our knowledge, the applicability and performance of such models in wine cellars have not yet been systematically analyzed. Accordingly, the objective of this study is to investigate how the unique structural and environmental features of underground wine cellars influence radio wave propagation, and to assess the suitability of existing propagation models for predicting attenuation in these environments.

In [16], we presented measurements of electric field strength in a basement environment with characteristics similar to a wine cellar, made for two frequencies, 860 MHz and 2.4 GHz. Those results were compared with predictions derived from the Free-Space (FS) propagation model [7], the tunnel propagation model [11], and the knife-edge diffraction model [13]. The present study extends this earlier research by performing measurements in two distinct basement environments, at three operating frequencies, and by comparing the results with seven existing propagation models.

The main contributions of this work are as follows:

- Radio wave propagation loss measurements were performed in two types of cellars, one semi-empty and one containing stainless-steel wine vessels, under both Line-of-Sight (LOS) and Non-Line-of-Sight (NLOS) conditions, at three frequencies: 860 MHz, 2400 MHz, and 3600 MHz.
- Seven propagation models, originally developed for environments with characteristics comparable to underground wine cellars, were analyzed and evaluated.
- The measured propagation losses and the corresponding values predicted by each model were compared, separately for LOS and NLOS conditions. Based on statistical analysis, the models that most accurately estimated losses as a function of the distance between the transmitter and receiver were identified, making them the most suitable for application in the design of radio networks in wine cellars.

The remainder of this paper is organized as follows. An overview of related work on modeling radio wave propagation in environments similar to underground wine cellars (tunnels, corridors, and street canyons) is provided in Section 2. Section 3 presents the experimental setup and measurement methodology. The propagation models used in this study are presented in Section 4, as well as a statistical analysis of the measurement results and propagation losses obtained by the propagation models. Finally, Section 5 provides the main conclusions of the study.

2. RELATED WORK

Radio wave propagation modeling in complex and confined environments has been the subject of extensive research, particularly in relation to emerging wireless technologies such as LoRa, NB-IoT, and 5G systems. Azevedo and Mendonça [23] provided a comprehensive critical review of propagation models employed in LoRa systems, identifying their suitability and limitations for different deployment scenarios. Their analysis found that most empirical models use logarithmic attenuation dependence on distance, as well as the need for environment-specific modeling, especially for NLOS conditions and constrained spaces. Similarly, Alobaidy et al [14] examined channel propagation models for IoT technologies, highlighting the challenges of achieving reliable wireless transmission in difficult conditions. These findings are consistent with broader studies on IoT and Industrial IoT (IIoT) communications, such as Ji-

ang et al. [13], who reviewed standardized 5G channel models for industrial environments, illustrating how 3GPP-defined frameworks can support next-generation industrial communications networks.

Over the years, a significant amount of research has been conducted on radio wave propagation in underground spaces and tunnels, environments that share physical and electromagnetic similarities with wine cellars. Emslie et al. [11] developed theoretical models for UHF propagation in coal mine tunnels, laying the foundation for subsequent empirical and semi-deterministic models for similar environments. Subrt and Pechac [18] proposed a semi-deterministic model for underground galleries and tunnels, while Rak and Pechac [24] analyzed UHF propagation in caves and underground passages, showing the influence of geometry and material properties on attenuation and multipath behavior. A comprehensive review by Hrovat et al. [20] and a more recent review by Samad et al. [19] provide systematic reviews of propagation modeling techniques in tunnel environments, including deterministic, empirical, and hybrid approaches. Empirical investigations of wireless sensor network (WSN) deployment in complex utility tunnels by Celaya-Echarri et al. [25] combined radio wave propagation analysis with network optimization methods. Li et al. [26] analyzed tunnel channels with human presence at 6 GHz, enhancing the understanding of body-induced multipath effects relevant to 5G communications.

Measurements in indoor environments provide further insight into modeling radio propagation in heterogeneous and obstructed spaces. Tan et al. [27] performed multipath delay measurements in multi-floor wireless communication scenarios. Similarly, Samad et al. [21] evaluated large-scale propagation models in indoor corridors at 3.7 and 28 GHz, validating their performance for 5G mobile network deployments.

Several studies have explored propagation in outdoor-to-deep-indoor settings relevant to underground industrial and agricultural facilities. Malarski et al. [28] and [29] investigated NB-IoT signal attenuation in deep-indoor conditions, providing empirical data on the importance of specific environmental features for sub-GHz signal strength prediction. Ali et al. [30] proposed a propagation loss model for neighborhood area networks in smart grids, integrating environmental variability into large-scale path loss estimation for an outdoor-to-deep-indoor scenario.

The propagation of radio waves in natural or artificial underground environments has also been examined through field measurements. Branch [31] conducted measurements of LoRa propagation in an underground gold mine and analyzed attenuation and multipath effects at 915 MHz. Soo et al. [15] investigated propagation behavior within a natural cave adapted for wine storage, providing one of the earliest studies linking radio wave propagation to wine cellar conditions. Together, these studies highlight the need for environment-specific propagation models tailored to the unique structural and material properties of cellars used in wine production

Although previous research has made significant progress in understanding the propagation of radio waves in various environments, including corridors and tunnels, the electromagnetic characterization of underground wine cellars remains insufficiently explored. The specific architectural features, high humidity levels, and presence of conductive storage vessels introduce propagation phenomena that differ from those observed in typical tunnel or building environments. These gaps motivate further efforts aimed at accurately characterizing the behavior of radio waves in wine cellars and optimizing wireless communication systems for smart wine production.

3. EXPERIMENTAL SETUP AND MEASUREMENT METHODOLOGY

The measurements were carried out in two different cellars. The first one, hereafter Cellar A, is the basement of a 19th-century building, completely built below ground level. This cellar is not used for wine production, but has all the architectural and environmental characteristics of a traditional underground wine cellar. Although it does not contain wine vessels, the space includes several wooden tables and shelves with metal components, as well as metal objects such as radiators and fire extinguishers (Fig. 1a). These objects are not typical of wine cellars, but their reflective and diffractive properties adequately mimic objects that similarly affect the propagation of radio waves in such environments.

Cellar A consists of six rooms (Fig. 1a), separated by brick walls approximately 74 cm thick. The ceiling is slightly arched, with a maximum height of 2.60 m at the center. At the beginning of the measurement campaign, the humidity in the basement was 65.3 %, and the temperature was 24.5 °C; by the end of the measurement, these values had dropped to 56.7 % and 21.8 °C due to additional ventilation. These conditions are typical for underground wine cellars, where high humidity inside the cellars indicates high humidity in the walls due to the porosity of the building material (brick, plaster) from which they are made [32]. The bricks' conductivity and relative dielectric permittivity, the quantities which determine the reflection coefficient, increase with the percentage of moisture [17, 33]. Consequently, this directly affects the power and phase shift of the reflected waves, and thus the total radio signal strength at the receiving site.

Measurements in Cellar A were carried out in rooms P1 and P6, with LOS propagation conditions achieved in P1 and NLOS in P6. The transmitting antenna was placed at the entrance to room P1 (marked with a star in Fig. 1a), and the measurement was carried out through the middle of the room at measurement points that were 0.5 m apart, starting from a distance of 1 m from

the transmitting antenna (the measurement locations are marked with dots in Fig. 1a).

The second facility, Cellar B, is an operational underground wine cellar of the Horvat Winery located in the Slavonija - Baranja County in eastern Croatia. Cellar B consists of a single elongated room containing 15 wine vessels of various sizes (Fig. 2a). The ceiling is slightly arched, with a maximum height of 3.18 m at the center. Ambient humidity and temperature were measured as 78.3 % and 18.7 °C, respectively. The measurement in Cellar B was carried out through the middle of the room, under LOS conditions of radio wave propagation.

The distance between the measurement points was also 0.5 meters, and their positions as well as the position of the transmitting antenna are shown in Fig. 2b, using the same notations as for Cellar A.

(a)

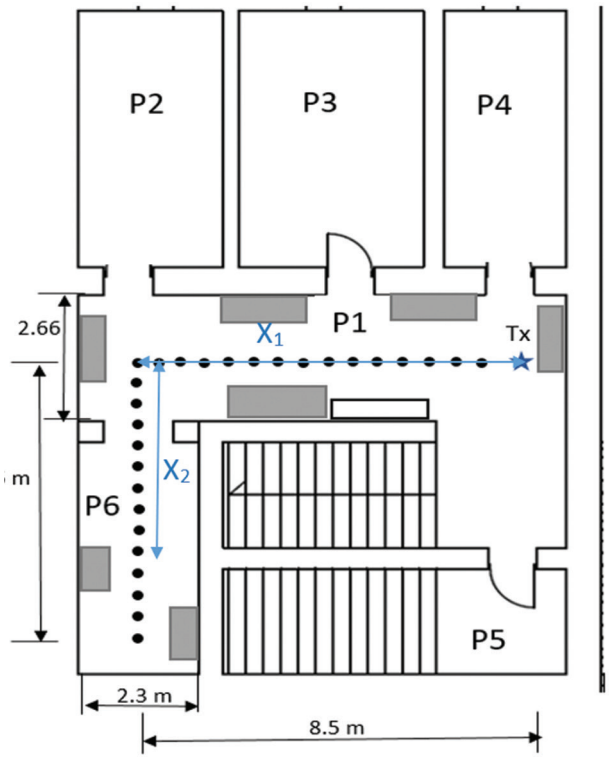

(b)

Fig. 1. a) Measurement setup in Cellar A; **b**) Cellar A plan

(a)

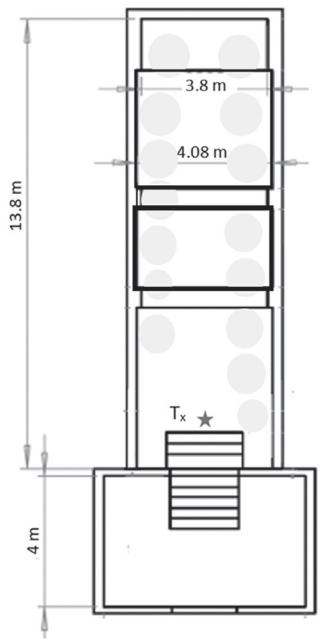

(b)

Fig. 2. a) Cellar B; **b**) Cellar B plan

The characteristics of Cellars A and B are summarized in Table 1.

Table 1. Architectural and environmental characteristics of the cellars

	Key characteristics of the cellars
Cellar A (Fig. 1)	• completely underground • 6 rooms, separated by 74 cm thick brick walls • several desks and shelves with metallic parts • LOS measurements in P1 and NLOS in P2 • P1 width W_{A1}=2.66 m, P2 width W_{A2}=2.33 m • arched ceiling with maximum height H_A=2.60m • humidity 56.7 % - 65.3 %, temperature 21.8 °C - 24.5 °C
Cellar B (Fig. 2)	• completely underground • 1 room, filled with large steel containers • LOS measurements • width W_B =4.08 m • arched ceiling with maximum height H_B=3.18m • humidity 78.3%, temperature 18.7°

Given the specific architectural and material features of both cellars, it was expected that signal strength at a given location would be significantly influenced by reflections from walls, ceilings, floors, and internal objects, as well as by diffraction at object edges and edges of walls at room transitions (particularly between P1 and P2 in Cellar A). Due to such multipath propagation, large variations in field strength can occur over small distances, even below $\lambda/2$. To mitigate these small-scale fluctuations, multiple measurements were taken within a circular area of 12 cm in diameter centered at each measurement location. The mean value of these measurements was used for further analysis.

To encompass most of the frequency bands used by Wi-Fi, LoRa, and NB-IoT systems, measurements were performed at 860 MHz, 2400 MHz, and 3600 MHz. Microwave signal generator ANA-PICO APSIN20G served as the transmitter, paired with vertically polarized dipole and logarithmic antennas, in dependence on frequency. A calibrated isotropic antenna Rhode&Schwarz TSEMF B1, and a spectrum analyzer Rhode&Schwarz FSH8 were used for electric field strength measurements. Detailed specifications of all equipment are provided in Table 2. Both the transmitting (Tx) and receiving (Rx) antennas were mounted on wooden tripods at a height of 1.5 m (Fig. 1a). The transmitter power was set to 15 dBm for all measurements.

The path loss (PL), expressed in decibels (dB), representing the attenuation of the radio wave between the Tx and Rx antennas, was calculated as:

$$PL[\mathrm{dB}] = P_{Tx}[\mathrm{dBW}] + G_{Tx}[\mathrm{dB}] - L_{cTx}[\mathrm{dB}] - (P_{Rx}[\mathrm{dBW}] + L_{cRx}[\mathrm{dB}] - G_{Rx}[\mathrm{dB}]) \quad (1)$$

P_{Tx} is the transmitter power, G_{Tx} and G_{Rx} are the antenna gains, L_{cTx} and L_{cRx} are cable losses, and P_{Rx} is received power. Antenna gains were derived from the antenna factors (AF) according to [34]:

$$G_{Tx}[\mathrm{dB}] = -149.7 + 20\log_{10} f[\mathrm{Hz}] - AF[\mathrm{dB/m}]. \quad (2)$$

Received power was computed from the measured electric field strength (E) using the following relations:

$$P_{Rx}[\mathrm{dBW}] = 10\log_{10}\frac{U^2}{R} = 10\log_{10}\frac{E^2}{AF_{lin}^2 R} \quad (3)$$

$$P_{Rx}[\mathrm{dBW}] = 20\log_{10}E[\mathrm{V/m}] - 20\log_{10}AF_{lin}[\mathrm{m^{-1}}] - 10\log_{10}R[\Omega] \quad (4)$$

or equivalently,

$$P_{Rx}[\mathrm{dBW}] = E[\mathrm{dBV/m}] - AF[\mathrm{dB/m}] - 10\log_{10}50 \quad (5)$$

Table 2. Experiment parameters

	Key data
Transmitter	Microwave signal generator ANA-PICO, APSIN20G P_{Tx} =15 dBm
Receiver	Spectrum analyzer ROHDE SCHWARZ FSH8
Operating frequencies	860 MHz, 2400 MHz and 3600 MHz
Transmitter antenna	Vertically polarized dipole antenna Seibersdorf Laboratories Precision Conical Dipole PCD 8250 for 860 MHz and 2400 MHz Vertically polarized antenna HyperLOG 30180 Aaronia for 3600 MHz
Receiver antenna	Isotropic antenna Rohde & Schwarz TSEMF B1 EMF Measurement Isotropic Probe
Extended uncertainty of measuring set	3.49 dB for f < 3 GHZ 3.99 dB for f ≥ 3 GHZ
Antenna height	h_{Tx} = 1.5 m, h_{Rx} = 1.5 m
Measurement points	28 at Cellar A, 21 at Cellar B 5-10 measurements at each measuring point - total of 560 and 315 measurements in cellar A and B, respectively

Cable losses and the receiving antenna factor were obtained from its calibration data, while the transmitting antenna factor was taken from [34].

For clarity, measurement results are expressed as path gain (PG), defined as the negative of path loss:

$$PG[\mathrm{dB}] = -PL[\mathrm{dB}] \quad (6)$$

Since path loss increases with distance, path gain correspondingly decreases, reflecting the reduction of received power as the receiver moves away from the transmitter.

4. PROPAGATION MODELS AND COMPARISON WITH MEASUREMENTS

4.1. RADIO WAVE PROPAGATION MODELS

We tested seven standardized propagation models for path loss prediction in underground wine cellars. For testing, we chose propagation models that were developed for environmental configurations similar to the characteristics of wine cellars.

The International Telecommunication Union Radiocommunication Sector (ITU-R) Recommendation ITU-R P.525-3, [7], provides the reference free-space propagation model, which is useful as a baseline for short-range links or to quantify the additional attenuation

introduced by the cellar environment. However, this model does not account for reflections, absorption, or scattering from walls and metallic objects, which are dominant effects in enclosed underground spaces. The formulas used in this paper for the free-space propagation loss model, as well as for the other path-loss models, are given in Table 3.

Indoor environments with corridor-like geometries are more appropriately represented by ITU-R P.1238-13, [8], which defines a site-general model for propagation in buildings and corridors. The vaulted structure and narrow passages of wine cellars closely resemble the conditions assumed in this recommendation, making it a suitable starting point for empirical path loss estimation. Nevertheless, parameter tuning is typically required, since ITU-R P.1238 is based on modern building materials rather than stone or brick walls typical of historic cellars.

The ITU-R P.1411-12, [9], site-general and site-specific models, originally developed for street-canyon propagation, can also be considered when the cellar exhibits elongated and narrow geometries. Namely, street-canyon propagation is characterized by multiple reflections from buildings and the ground that cause a waveguide effect, which can also be expected for long basement corridors.

Since wine cellars contain large steel wine tanks, the radio wave propagation conditions could be similar to those in industrial buildings. To investigate this, we have considered the site-general model for indoor propagation in factory environments with dense clutter and low base station heights, defined in ETSI TR 138 901 V16.1.0, [10]. The higher path loss exponents and increased shadowing predicted by this model are consistent with environments dominated by large reflective objects and strong multipath components.

The tunnel propagation model, originally proposed by Emslie et al. [11], describes the behavior of UHF (Ultra High Frequency) radio waves in tunnel-like environments where multiple reflections from the walls, floor, and ceiling create a waveguiding effect. The model divides propagation into two regions: a free-space region close to the transmitter and a waveguide region beyond the Fresnel breakpoint distance, where attenuation increases approximately linearly with distance. This formulation effectively captures the transition from spherical to guided propagation and has since been widely applied to model radio wave behavior in underground and enclosed environments with elongated geometries.

In addition, ITU-R P.526-14 [12], which describes the classical knife-edge diffraction method, is relevant for modeling wave propagation at transitions between rooms, doorways, or the edges of large metallic containers. In such cases, diffraction losses can be estimated separately and combined with the baseline statistical model to improve prediction accuracy.

4.2. PROPAGATION MODELS VS. MEASUREMENTS

The measurement results are presented in terms of path gain, calculated using the equations described in Section 3. The electric field strength at each measurement point represents the mean of five to ten measurements taken within a circular area of 12 cm in diameter centered on that point. Accordingly, the reported results show the average path gain as a function of the distance between the transmitting and receiving antennas. Table 4 lists the standard deviations of the individual measurements related to their respective mean values, which range from 2.09 dB to 3.06 dB, indicating the level of the field strength variations in that small area.

The measurement results for both cellars are presented in Fig. 3. In each case, the path gain decreases with increasing frequency, as expected. A pronounced reduction in path gain is also evident in Cellar A within the NLOS region.

A direct comparison between Cellar A and Cellar B is possible only under LOS conditions, i.e., for all points in Cellar B and up to 9 m in Cellar A. The steel wine containers in Cellar B were expected to cause stronger attenuation. This was confirmed at 2.4 GHz, where the average field strength in Cellar B was 4.3 dB lower than in Cellar A. At 860 MHz, however, the difference was only 1.4 dB, likely due to the longer wavelength and weaker interaction of the wave with metallic surfaces.

Propagation was also influenced by transmitter antenna placement. In Cellar A, the transmitter was located 1 m from a brick wall, with openings to adjacent rooms on both sides. In Cellar B, it was positioned near a wide opening to another chamber, bounded laterally by a wall and a metal wine container. These geometric differences contributed to the observed variation in path gain.

Measured path gains are compared with the theoretical free-space model in Fig. 3. In Cellar B, the agreement at a 1 m Tx–Rx separation is within 1 dB. In Cellar A, measured path gains at distance of 1 m exceed free-space predictions by 2.7 dB at 860 MHz, 4.3 dB at 2.4 GHz, and 4.2 dB at 3.6 GHz, primarily due to reflections from nearby surfaces. For larger distances, the free-space model significantly overestimates path loss in both cellars, confirming the strong effects of multipath propagation and absorption in enclosed environments.

In addition to the free-space propagation model, the measured path gain results were compared with the predictions obtained from six additional propagation models, which can be categorized into two groups.

The first group comprises site-general models, which incorporate environmental characteristics indirectly through empirical parameters α, β, and γ, fitted for the type of environment under consideration. These parameters appear in the general path loss formulation

$$PL(d,f) = 10\alpha \cdot \log_{10}(d) + \beta + 10\gamma \cdot \log_{10}(f) \quad (7)$$

Table 3. Selected propagation path-loss models

Propagation model	LOS/ NLOS	Path loss, PL (dB) (f is in GHz, d is in m)	Shadow fading std (dB)	Frequency range (GHz)	Distance range (m)
ITU-R P.525-3 Free space model, [7]	LOS	$PL_{FS}(d,f) = 92.4 + 20 \cdot \log_{10}(d) + 20 \cdot \log_{10}(f)$			
ITU-R P.1238-13 Site-general model for propagation in corridors, [8]	LOS	$PL_b(d,f) = 15.7 \cdot \log_{10}(d) + 29.46 + 22.4 \cdot \log_{10}(f)$	σ=3.77	0.3-300	2-160
	NLOS	$PL_b(d,f) = 27.8 \cdot \log_{10}(d_{3D}) + 28.62 + 25.4 \cdot \log_{10}(f)$	σ=7.58	0.625-159	3-94
ITU-R P.1411-12 Site-general model for propagation within street canyons, [9]	LOS	$PL_b(d,f) = 21.2 \cdot \log_{10}(d) + 29.2 + 21.1 \cdot \log_{10}(f)$	σ=5.06	0.8-82	5-660
	NLOS	$PL_b(d,f) = 40 \cdot \log_{10}(d) + 10.2 + 23.6 \cdot \log_{10}(f)$	σ=7.6	0.8-82	30-715
ITU-R P.1411-12 Site-specific model for propagation within street canyons, [9]	LOS	$PL_{LOS,m} = L_{bp} + 6 + \begin{cases} 20 \cdot log_{10}\left(\frac{d}{R_{bp}}\right) & for\ d \le R_{bp} \\ 40 \cdot log_{10}\left(\frac{d}{R_{bp}}\right) & for\ d > R_{bp} \end{cases}$ $L_{bp} = 10 \cdot \log_{10}\left\lvert\frac{\lambda^2}{8\pi h_1 h_2}\right\rvert \quad R_{bp} \approx \frac{4h_1h_2}{\lambda}$		0.3-3	
	NLOS	$PL_{NLOS2} = 10 \cdot \log_{10}(10^{-\frac{L_r}{10}} + 10^{-\frac{L_d}{10}})$ $L_r = 20\log_{10}(x_1 + x_2) + x_1 \cdot x_2 \frac{f(\alpha)}{W_1 W_2} + 20\log_{10}\left(\frac{4\pi}{\lambda}\right)$ $f(\alpha) = \frac{3.86}{\alpha^{3.5}} \quad 0.6 < \alpha(\text{rad}) < \pi$ $L_d = 10\log_{10}(x_1 x_2 (x_1 + x_2) + 2D_a - 0.1\left(90 - \alpha\frac{180}{\pi}\right) + 20\log_{10}\left(\frac{4\pi}{\lambda}\right)$ $D_a = \frac{40}{2\pi}\left[\arctan\left(\frac{x_1}{W_1}\right) + \arctan\left(\frac{x_2}{W_2}\right) - \frac{\pi}{2}\right]$ $PL_{NLOS2} = L_{LOS} + L_c + L_{att}$ $L_c = \begin{cases} \frac{L_{corner}}{\log_{10}(1 + d_{corner})}\log_{10}\left(x_2 - \frac{W_1}{2}\right) & \frac{W_1}{2} + 1 < x_2 \le \frac{W_1}{2} + 1 + d_c \\ L_{corner} & x_2 > \frac{W_1}{2} + 1 + d_{corner} \end{cases}$ $L_{att} = \begin{cases} 60\log_{10}\left(\frac{x_1 + x_2}{x_1 + \frac{W_1}{2} + d_{corner}}\right) & x_2 > \frac{W_1}{2} + 1 + d_{corner} \\ 0 & x_2 \le \frac{W_1}{2} + 1 + d_{corner} \end{cases}$		0.8-2 2-28	
ETSI TR 138 901 V16.1.0 Site-general model for indoor propagation in factory with dense clutter and low BS (InF-DL), [10]	LOS	$PL_b(d,f) = 21.5 \cdot \log_{10}(d) + 31.84 + 19 \cdot \log_{10}(f)$	σ=4	0.5-100	1-600
	NLOS	$PL_b(d,f) = 35.7 \cdot \log_{10}((d_{3D})) + 18.6 + 20 \cdot \log_{10}(f)$	σ=7.2	0.5-100	1-600
Tunnel model, [11]	LOS	$PL_{Tunnel}(d) = \begin{cases} L_{FS}(d) & for \quad d < d_{BP} \\ L_{FS}(d_{BP}) + \alpha \cdot (d_{BP} - d) & for \quad d \ge d_{BP} \end{cases}$ $\alpha = 5.13 \cdot \lambda^2 \cdot \left(\frac{1}{W^3\sqrt{\varepsilon_v - 1}} + \frac{\varepsilon_h}{H^3\sqrt{\varepsilon_h - 1}}\right), \quad d_{BP} = \frac{4(H - h_A)^2}{\lambda}$			
ITU-R P.526-14 Knife-edge diffraction model, [12]	NLOS	$PL_d = 6.9 + 20\log_{10}(\sqrt{(\nu - 0.1)^2 + 1} + \nu - 0.1 \quad \text{for } \nu > -0.78$ $\nu = h\sqrt{\frac{2}{\lambda}\frac{d_2 + d_1}{d_1 d_2}}$			

Although these models account for the specific type of environment (e.g., indoor, urban, or suburban), they do not explicitly consider the geometric properties of that environment (see Table 3).

Conversely, site-specific models explicitly incorporate geometric parameters of the propagation environment (such as street width, tunnel height, and tunnel width) into the path loss computation.

Fig. 4 presents the measurement results alongside the path loss values predicted by the site-general models ITU-R P.1238-13, ITU-R P.1411-12 (site-general), and ETSI TR 138 901 V16.1.0.

Among these, the ITU-R P.1238-13 model demonstrated the closest agreement with the measured data, while the other models tended to overestimate path losses. The ITU-R P.1238-13 model provided an accu-

rate estimate of losses in LOS region, yielding an average Root Mean Squared Error (RMSE) of 2.8 dB (Table 5). In NLOS region, however, the error increased significantly to 12.37 dB (Table 6). This is to be expected, as the model is designed for indoor propagation in buildings, where in NLOS areas, significant signal strength comes from wave components passing through walls. In Cellar A, for NLOS measurement points in room P2, radio waves need to penetrate two 74 cm thick walls and propagate partially through the ground.

The results obtained from the site-specific models—namely ITU-R P.1411-12 (site-specific), the tunnel model, and the ITU-R P.526-14 (knife-edge diffraction) model—are illustrated in Fig. 5.

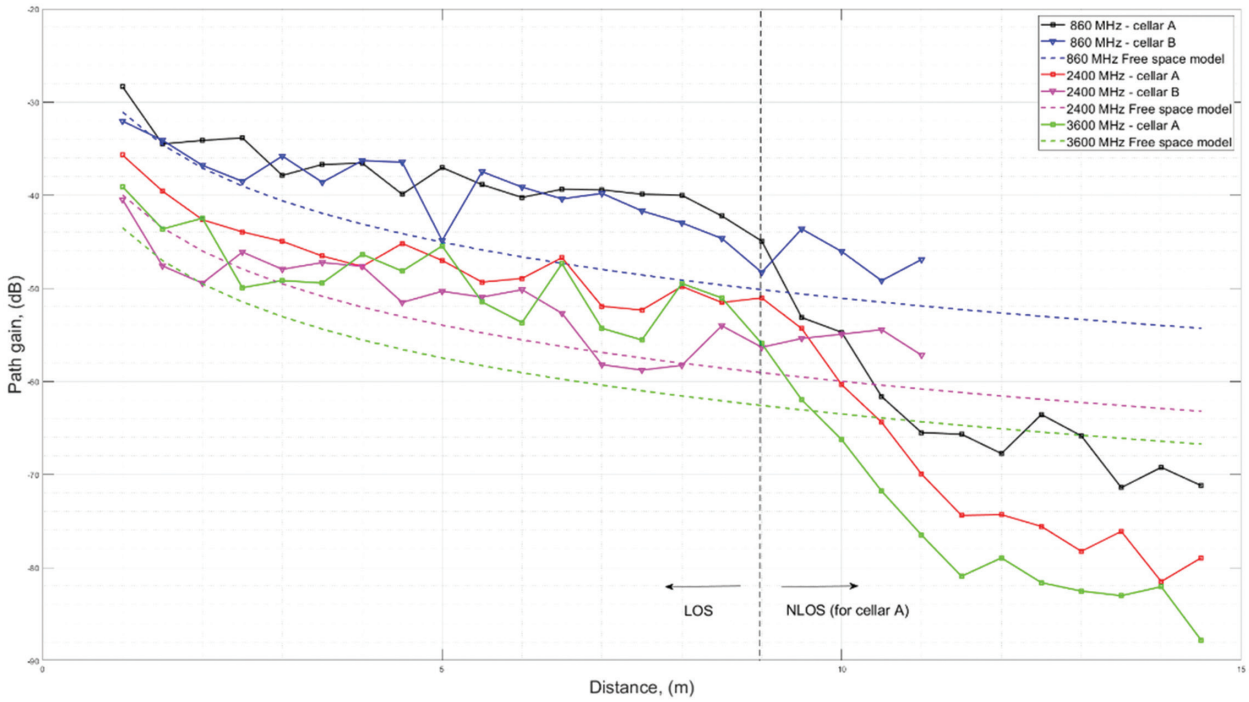

Fig. 3. Results of measurements in Cellar A and Cellar B presented as Path gain in dB

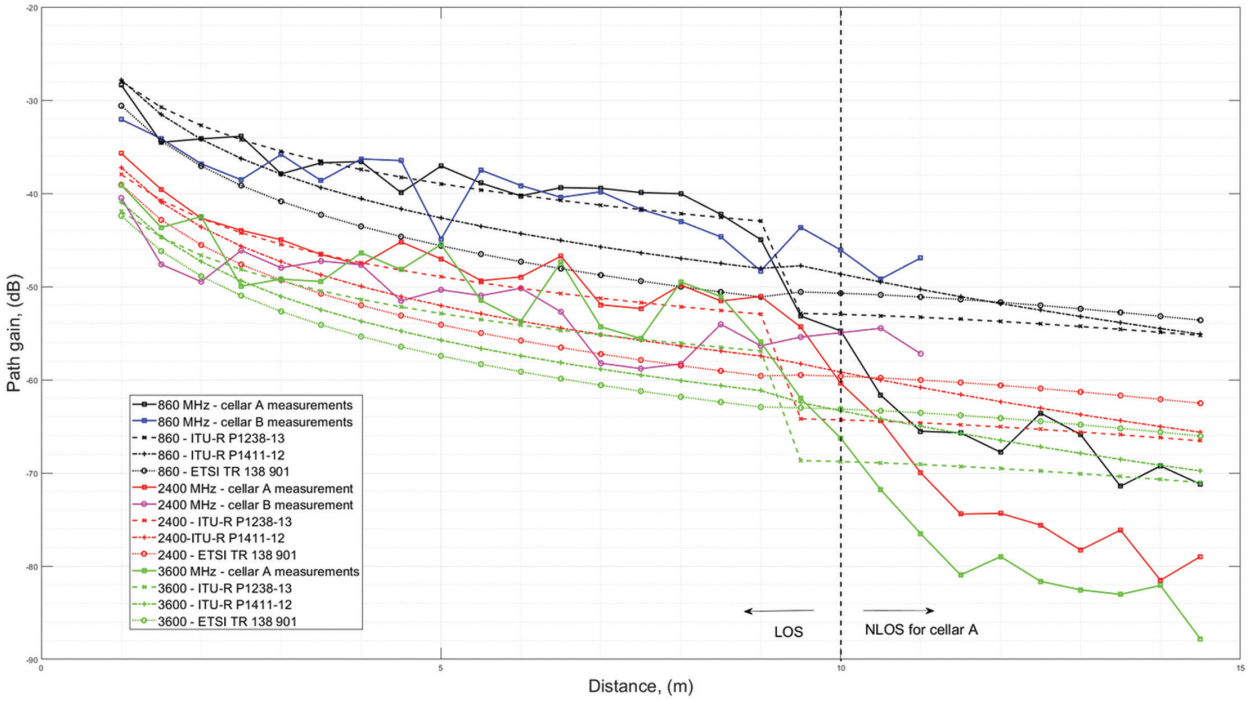

Fig. 4. Comparison of measured results and site-general models' ITU-R P.1238-13, ITU-R P.1411-12 (site-general), and ETSI TR 138 901 V16.1.0. results

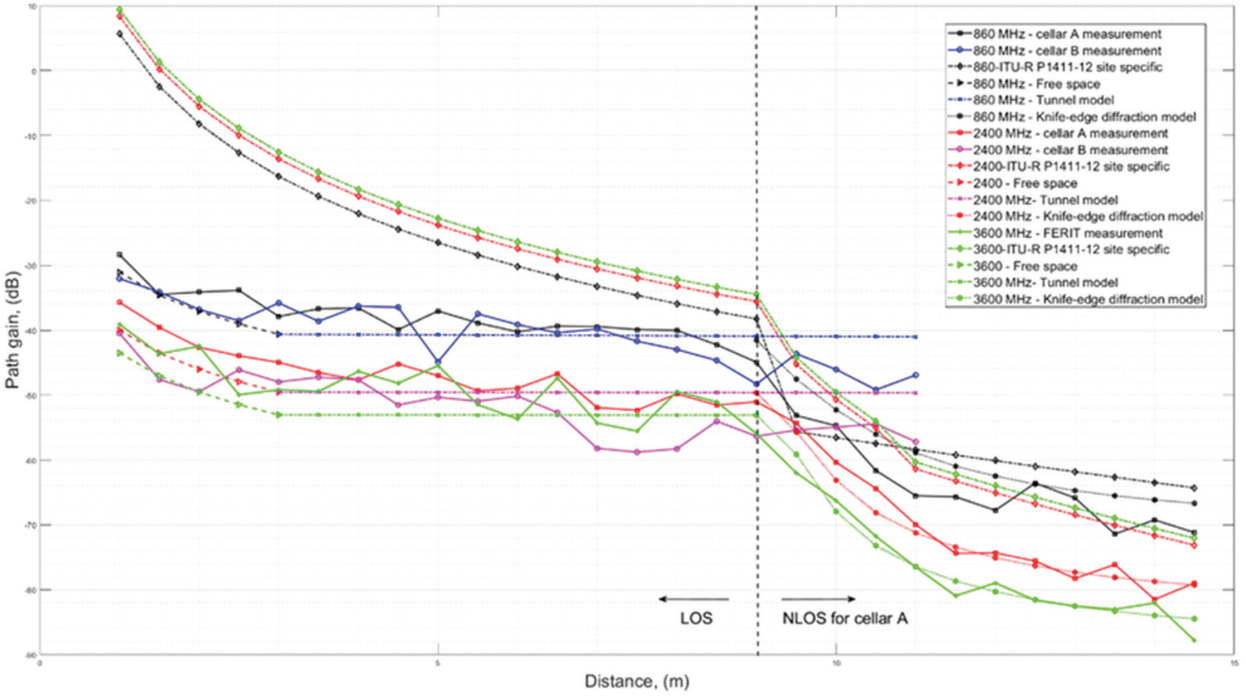

Fig. 5. Comparison of measured results and site-specific ITU-R P.1411-12 (site-specific) model, the tunnel model, and the ITU-R P.526-14 (knife-edge diffraction) model results

Table 4. Standard deviations of the individual measurements from their respective mean values

Measurements standard deviation				
860 MHz		2400 MHz		3600 MHz
Cellar A	Cellar B	Cellar A	Cellar B	Cellar A
2.79 dB	2.14 dB	3.06 dB	2.99 dB	2.09 dB

Table 5. RMSE for different models against measurement results for LOS propagation

LOS conditions	RMSE [dB]					
	860 MHz		2400 MHz		3600 MHz	Average
	Cellar A	Cellar B	Cellar A	Cellar B	Cellar A	
Free space model (FS)	6.20	5.35	6.07	3.52	7.79	5.79
ITU-R P.1238-13	1.66	2.99	1.69	3.74	3.90	2.80
ITU-R P.1411-12 Site-general	4.26	3.77	4.29	3.04	6.26	4.32
ETSI TR 138 901 V16	6.83	5.96	6.17	3.82	7.74	6.10
ITU-R P.1411-12 Site-specific	17.26	16.94	27.40	29.50	30.87	24.39
FS+Tunnel	2.83	3.18	2.95	4.61	4.25	3.56
Fitted model	1.42	2.44	1.30	2.29	2.65	2.02

The tunnel model was applied exclusively to the LOS region, while the knife-edge diffraction model was applied to the NLOS region, consistent with their respective domains of validity.

The tunnel model predicts propagation behavior consistent with the free-space model up to a distance shorter than the Fresnel breakpoint distance, d_{BP} (Table 3). For Cellar A, d_{BP} = 13.9 m, and for Cellar B, d_{BP} = 32.4 m at 860 MHz; at higher frequencies (2.4 GHz and 3.6 GHz), the breakpoint distances are even greater.

However, the measurement results indicate that the tunnel effect, characterized by a slow increase in path loss with distance, occurs much earlier, at approximately 2 – 2.5 m. Consequently, the tunnel model results in Fig. 5 were adjusted by setting d_{BP} = 2.5 m to better align with empirical observations. To calculate the α parameter for this model, we used $\varepsilon_h = \varepsilon_v = 3.75$, which corresponds to the values for bricks according to [35].

Table 6. RMSE for different models against measurement results for NLOS propagation

NLOS conditions	RMSE [dB]			
	860 MHz	2400 MHz	3600 MHz	Average
	Cellar A	Cellar A	Cellar A	
ITU-R P.1238-13	11.84	9.90	10.47	10.74
ITU-R P.1411-12 Site-general	13.42	11.22	12.47	12.37
ETSI TR 138 901 V16	13.62	13.12	14.89	13.88
ITU-R P.1411-12 Site-specific	5.71	8.99	28.99	14.56
Knife-edge diffraction	4.56	1.98	1.78	2.77
Fitted model	2.54	2.76	2.64	2.65

Further adjustments were made to the ITU-R P.1411-12 (site-specific) model based on the measurement data. Specifically, it was observed that the parameter d_{corner}, which denotes the transition zone between LOS and NLOS regions and where the path gain decreases by 20 dB, corresponds to the width of room P2. This width is 2.5 m, substantially smaller than the 30 m specified in the original model. The ITU-R P.1411-12 model was originally developed for urban street canyon environments, where 30 m represents an average street width. By analogy, for propagation within Cellar A, the width of room P2 serves as the corresponding environmental parameter governing the LOS-to-NLOS transition.

It should be noted that in Fig. 3-6, within the NLOS region, the distance (d) between the transmitter (Tx) and each measurement point is expressed as the sum of two components, X_1 and X_2, as illustrated in Fig. 1(b). Specifically, $X_1 = 8.5$ m represents the distance from the transmitter to the last measurement point located in room P1, while X_2 denotes the distance from that point to the corresponding measurement position in room P2. For propagation models in which the path loss is defined as a function of the three-dimensional distance d_{3D} this distance is computed as follows:

$$d_{3D} = \sqrt{X_1^2 + X_2^2 + \Delta h^2} \tag{8}$$

where Δh presents the height difference between the transmitting and receiving antennas.

For the site-specific propagation models, the tunnel model for LOS region and the knife-edge diffraction model for NLOS region yielded the most accurate results, with RMSE of 3.56 dB and 2.77 dB, respectively. As shown in Fig. 5, the tunnel model accurately predicts the average path gain variation up to a distance of 7 meters at 860 MHz for both basement environments. However, for longer distances in Cellar B, the model tends to overestimate the path gain. In Cellar A, the model also provides good agreement with measurements at 2.4 GHz, whereas in other scenarios the discrepancy between measured and predicted values increases substantially (RMSE > 4.2 dB).

The knife-edge diffraction model performs well at 2400 MHz and 3600 MHz, achieving RMSE values below 2 dB, while at 860 MHz the RMSE increases to 4.56 dB. Part of this error at 860 MHz stems from inaccuracies in the tunnel model's path gain estimate at a distance of 9 meters, which serves as the initial condition for the knife-edge diffraction model's calculation.

In contrast, the ITU-R P.1411-12 site-specific model exhibits significantly higher prediction errors. In the LOS region, the average RMSE is approximately 24 dB, and the model even predicts positive path gains within 2 meters of the transmitter—a physically implausible outcome. For the NLOS region, the RMSE reaches 14.56 dB, largely due to the over 6 dB error in the LOS path gain at 9 meters, which propagates into the NLOS region calculations since this value is used as the initial reference.

The final comparison was by fitting the coefficients α, β, and γ of the path-loss model (6) to the measurement results using least-squares regression. We compared the obtained with the corresponding coefficients in the general-site models. The results of the fitted models are presented in Fig. 6, and the corresponding coefficients are summarized in Table 7. For reference, Table 7 also includes the coefficient values defined in the site-general models: Free-Space model, ITU-R P.1238-13, ITU-R P.1411-12 (site-general), and ETSI TR 138 901 V16.1.0. models.

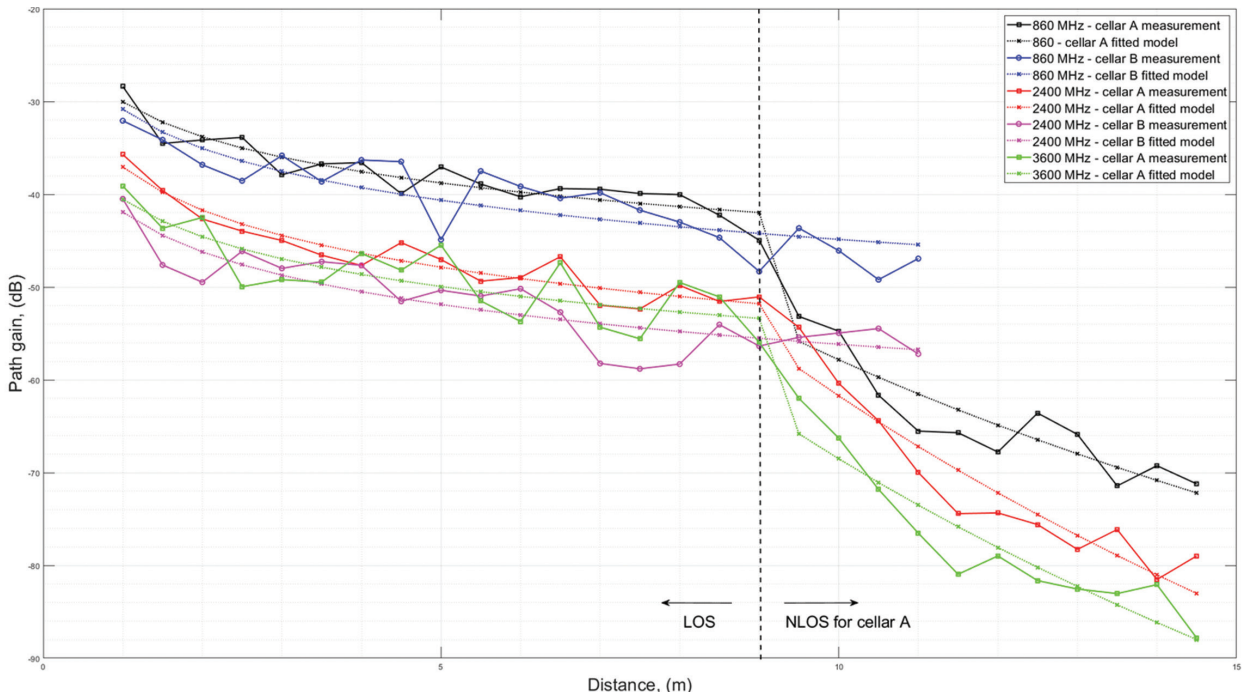

Fig. 6. Measurement results and results of corresponding fitted models

Table 7. Comparison of propagation model parameters

		Parameters for the model $PL(d, f)=10\alpha\cdot\log_{10}(d)+\beta+10\gamma\cdot\log_{10}(f)$					
		LOS			NLOS		
		α	β	γ	α	β	γ
Free space model		2	92.4	2	-	-	-
ITU-R P.1238-13		1.57	29.46	2.24	2.78	28.62	2.54
ITU-R P.1411-12 Site-general		2.12	29.2	2.11	4	10.2	2.36
ETSI TR 138 901 V16		2.15	31.84	1.9	3.57	18.6	1.9
Fitted models A	860 MHZ	1,25	31.68	1.66	8.9	-31.14	-
	2400 MHz	1.54	31.68	1.66	13.2	-70.29	-
	3600 MHz	1.35	31.68	1.66	12.01	-52.22	-
Fitted models B	860 MHZ	1.4	31.68	1.66	-	-	-
	2400 MHz	1.42	31.68	1.66	-	-	-

Under line-of-sight (LOS) conditions, the fitted coefficients were found to be in the ranges α = 1.25 - 1.54, β = 31.68, and γ = 1.66. These values are closest to those specified in the ITU-R P.1238-13 model, corroborating its strong predictive performance. For NLOS conditions, the fitted coefficients vary considerably, with α = 8.9-13.2, β = -31.14 – (-70.29), while γ could not be determined. These values differ substantially from those in the corresponding site-general models, highlighting their inadequacy for accurate prediction in NLOS environments.

The average RMSE of the fitted models is 2.02 dB for LOS and 2.65 dB for NLOS conditions (Tables 5 and 6).

5. CONCLUSIONS

This paper presents the results of path loss measurements of radio waves in underground wine cellars to assess the applicability of existing propagation models for IoT-based monitoring and control systems in smart wineries. The measurements were performed at frequencies 860 MHz, 2400 MHz, and 3600 GHz under LOS and NLOS conditions in two different cellar environments, one semi-empty and one filled with metal wine containers.

By comparing measurement results with the path loss values predicted by seven propagation models, it was found that for LOS conditions, the ITU-R P.1238-13 model and the tunnel model provide the most accurate predictions. The ITU-R P.1238-13 model achieved an average RMSE of 2.8 dB, while the tunnel model provided comparable accuracy (average RMSE = 3.56 dB), showing that these models successfully capture the dominant mechanisms of radio wave propagation in elongated basement spaces.

For NLOS conditions, the knife-edge diffraction model achieved the best correspondence with experimental data, with an average RMSE of 2.77 dB. In contrast, the site-specific ITU-R P.1411-12 model exhibited large deviations and physically inconsistent results, indicating its limited applicability to underground cellars.

Using least squares regression, coefficients for a general path-loss model fitted to the measurement data were obtained, which achieved average RMSE values of 2.02 dB (LOS) and 2.65 dB (NLOS). The obtained model coefficients closely match the parameters of the ITU-R P.1238-13 model for LOS conditions, confirming its applicability to basement environments.

It can be concluded that a hybrid modeling approach, i.e., a combination of the ITU-R P.1238-13 or tunnel model for LOS and a diffraction-based model for NLOS conditions, offers the most reliable and physically based prediction of path loss in underground wine cellars. This approach enables accurate signal estimation for low-power IoT communication systems such as LoRa, NB-IoT, and Wi-Fi, providing a practical basis for the application of smart production process monitoring technologies in the wine industry.

In future work, we plan to investigate some aspects of the presented research further. Given that in real wireless sensor networks antennas are not isotropic, as the receiving antenna used in our measurements, it can be expected that some correction/offset is required for the model. The necessity for the correction is expected both in the path loss estimation and in the field strength standard deviation.

Namely, an isotropic antenna captures reflections and diffractions from all directions, in contrast to real IoT antennas that are directional and have specific polarization. The impact of different transmitting antennas on path losses in such a complex environment could also be investigated.

Another aspect worth considering is how well wireless network planning simulation tools can estimate propagation for spaces as underground wine cellars. Modeling such spaces, considering their geometry and the electrodynamic properties of the building materials in conditions of increased humidity, presents a particular challenge.

ACKNOWLEDGMENT

This work results from implementing research activities on the project Development of an expert system for food production and processing management (ESIA-Expert System for Intelligent Agriculture) KK.01.1.1.07.0036 funded by the European Regional Development Fund.

The authors would like to thank Ivana Kovačević, Robert Miling, and Ivan Vučina for their support and assistance during the measurements.

6. REFERENCES:

[1] S. Kontogiannis, M. Tsoumani, G. Kokkonis, C. Pikridas, Y. Kotseridis, "Proposed SmartBarrel System for Monitoring and Assessment of Wine Fermentation Processes Using IoT Nose and Tongue Devices", Sensors, Vol. 25, No. 13, 2025.

[2] J. Nelson, R. Boulton, A. Knoesen, "Automated Density Measurement with Real-Time Predictive Modeling of Wine Fermentations", IEEE Transactions on Instrumentation and Measurement, Vol. 71, 2022, pp. 1-7.

[3] D. Oreški, I. Pihir, K. Cajzek, "Smart Agriculture and Digital Transformation on Case of Intelligent System for Wine Quality Prediction", Proceedings of the 44th International Convention on Information, Communication and Electronic Technology, Opatija, Croatia, 27 September - 1 October 2021, pp. 1370-1375.

[4] I. Kovačević, M. Orić, I. Hartmann Tolić, E. K. Nyarko, "Modelling the Fermentation Process in Winemaking using Temperature and Specific Gravity", Proceedings of the Central European Conference on Information And Intelligent Systems, Dubrovnik, Croatia, 20-22 September 2023, pp. 347-352.

[5] I. Kovačević, I. Aleksi, T. Keser, T. Matić, "Winnie: A Sensor-Based System for Real-Time Monitoring and Quality Tracking in Wine Fermentation", Applied Sciences, Vol. 15, No. 21, 11317, 2025.

[6] G. Masetti, F. Marazzi, L. Di Cecilia, L. Rovati, "IOT-Based Measurement System for Wine Industry", Proceedings of Workshop on Metrology for Industry 4.0 and IoT, Brescia, Italy, 16-18 April 2018, pp. 163-168.

[7] ITU-R P.525-3 Calculation of Free-space Attenuation, International Telecommunication Union – Radiocommunication Sector (ITU-R), Geneva, Switzerland, 2019.

[8] ITU-R P.1238-13 Propagation Data and Prediction Methods for the Planning of Indoor Radiocommunication Systems and Radio Local Area Networks in the Frequency Range 300 MHz to 450 GHz, International Telecommunication Union – Radiocommunication Sector (ITU-R), Geneva, Switzerland, 2023.

[9] ITU-R P.1411-12 Propagation Data and Prediction Methods for the Planning of Short-Range Outdoor Radiocommunication Systems and Radio Local Area Networks in the Frequency Range 300 MHz to 100 GHz, International Telecommunication Union – Radiocommunication Sector (ITU-R), Geneva, Switzerland, 2023.

[10] ETSI TR 138 901 V16.1.0 Study on channel model for frequencies from 0.5 to 100 GHz (3GPP TR 38.901 version 16.1.0 Release 16), European Telecommunications Standards Institute (ETSI), Sophia Antipolis, France, 2020

[11] A. Emslie, R. Lagace, P. Strong, "Theory of the Propagation of UHF Radio Waves in Coal Mine Tunnels", IEEE Transactions on Antennas and Propagation, Vol. 23, No. 2, 1975, pp. 192-205.

[12] ITU-R.526-14 Propagation by Diffraction, International Telecommunication Union - Radiocommunication Sector (ITU-R), Geneva, Switzerland, 2018.

[13] T. Jiang, J. Zhang, P. Tang, L. Tian, Y. Zheng, J. Dou, H. Asplund, L. Raschkowski, R. D'Errico, T. Jämsä, "3GPP Standardized 5G Channel Model for IIoT Scenarios: A Survey", IEEE Internet of Things Journal, Vol. 8, No. 11, 2021, pp. 8799-8815.

[14] H. A. H. Alobaidy, M. Jit Singh, M. Behjati, R. Nordin, N. F. Abdullah, "Wireless Transmissions, Propagation and Channel Modelling for IoT Technologies: Applications and Challenges", IEEE Access, Vol. 10, 2022, pp. 24095-24131.

[15] Q. P. Soo, S. Y. Lim, D. W. G. Lim, K. M. Yap, S. L. Lau, "Propagation Measurement of a Natural Cave-turned-wine-cellar", IEEE Antennas and Wireless Propagation Letters, Vol. 17, No. 5, 2018, pp. 743-746.

[16] S. Rimac-Drlje, S. Rupčić, T. Keser, I. Kovačević, R. Miling, V. Mandrić, "Propagation of Radio Waves in Wine Cellars", Proceedings of 30th International Conference on Systems, Signals and Image Processing, Ohrid, North Macedonia, 27-29 June 2023, pp. 1-5.

[17] L. Mollo, R. Greco, "Moisture Measurements in Masonry Materials by Time Domain Reflectometry", Journal of Materials in Civil Engineering, Vol. 23, No. 4, 2011, pp. 441-444.

[18] L. Subrt, P. Pechac, "Semi-Deterministic Propagation Model for Subterranean Galleries and Tunnels", IEEE Transactions on Antennas and Propagation, Vol. 58, No. 11, 2010, pp. 3701-3706.

[19] M. A. Samad, S. W. Choi, C. S. Kim, K. Choi, "Wave Propagation Modeling Techniques in Tunnel Environments: A Survey", IEEE Access, 2023, Vol. 11, 2023, pp. 2199-2225.

[20] A. Hrovat, G. Kandus, T. Javornik, "A Survey of Radio Propagation Modeling for Tunnels", IEEE Communications Surveys and Tutorials, Vol. 16, No. 2, 2014, pp. 658-669.

[21] M. A. Samad, F. D. Diba, Y. J. Kim, D. Y. Choi, "Results of Large-Scale Propagation Models in Campus Corridor at 3.7 and 28 GHz", Sensors, Vol. 21, No. 22, 2021.

[22] Z. Changsen, M. Yan, "Effects of Cross Section of Mine Tunnel on the Propagation Characteristics of UHF Radio Wave", Proceedings of the 7th International Symposium on Antennas, Propagation & EM Theory, Guilin, China, 26-29 October 2006, pp. 1-5.

[23] J. A. Azevedo, F. Mendonça, "A Critical Review of the Propagation Models Employed in LoRa Systems", Sensors, Vol. 24, No. 12, 2024.

[24] M. Rak, P. Pechac, "UHF Propagation In Caves And Subterranean Galleries", IEEE Transactions on Antennas and Propagation, Vol. 55, No. 4, 2007, pp. 1134-1138.

[25] M. Celaya-Echarri, L. Azpilicueta, P. Lopez-Iturri, I. Picallo, E. Aguirre, J. J. Astrain, J. Villandagos, F. Falcone, "Radio Wave Propagation and WSN Deployment in Complex Utility Tunnel Environments", Sensors, Vol. 20, No. 23, 2020.

[26] S. Li, Y. Liu, L. Lin, W. Ji, Z. Zhu, "Measurement, Simulation and Modeling in the Tunnel Channel with Human Bodies at 6 GHz for 5G Wireless Communication System", Proceedings of the 12th International Symposium on Antennas, Propagation and EM Theory, Hangzhou, China, 3-6 December 2018, pp. 1-4.

[27] S. Y. Tan, M. Y. Tan, H. S. Tan, "Multipath Delay Measurements and Modeling for Interfloor Wireless Communications", IEEE Transactions on Vehicular Technology, Vol. 49, No. 4, 2000, pp. 1334-1341.

[28] K. M. Malarski, J. Thrane, M. G. Bech, K. Macheta, H. L. Christiansen, M. N. Petersen, and S. Ruepp "Investigation of Deep Indoor NB-IoT Propagation Attenuation", Proceedings of the IEEE 90th Vehicular Technology Conference, Honolulu, HI, USA, 22-25 September 2019, pp. 1-5.

[29] K. M. Malarski, J. Thrane, H. L. Christiansen, S. Ruepp, "Understanding Sub-GHz Signal Behavior in Deep-Indoor Scenarios", IEEE Internet of Things Journal, Vol. 8, No. 8, 2021, pp. 6746-6756.

[30] M. B. Ali, W. Endemann, R. Kays, "Propagation Loss Model for Neighborhood Area Networks in Smart Grids", Journal of Communications and Networks, Vol. 24, No. 3, 2022, pp. 313-323.

[31] P. Branch, "Measurements and Models of 915 MHz LoRa Radio Propagation in an Underground Gold Mine", Sensors, Vol. 22, No. 22, 2022.

[32] D. D'Ayala, Y. D. Aktas, "Moisture Dynamics in the Masonry Fabric of Historic Buildings Subjected to Wind-Driven Rain and Flooding", Building and Environment, Vol. 104, 2016, pp. 208-220.

[33] R. Agliata, T. A. Bogaard, R. Greco, L. Mollo, E. C. Slob, S. C. Steele-Dunne, "Non-invasive estimation of moisture content in tuff bricks by GPR", Construction and Building Materials, Vol. 160, 2018, pp. 698-706.

[34] Z. Živković, A. Šarolić, "Measurements of Antenna Parameters in GTEM Cell", Journal of Communications Software and Systems, Vol. 6, No. 4, 2010, pp. 125-132.

[35] ITU-R, "Recommendation ITU-R P.2040-1 Effects of Building Materials and Structures on Radiowave Propagation Above About 100 MHz, P Series Radiowave propagation", 2015.